Quantitative Correlation of Raman Spectral Indicators in Determining Conformational Order in Alkyl Chains

Christopher J. Orendorff, Michael W. Ducey, Jr.,† and Jeanne E. Pemberton*

University of Arizona, Department of Chemistry, 1306 East University Blvd., Tucson, Arizona 85721

Received: November 26, 2001; In Final Form: May 28, 2002

The correlation of Raman spectral indicators for the determination of alkyl chain interactions and conformational order is presented. These investigations probe the conformational order of bulk octadecane and low molecular weight polyethylene as they undergo solid/liquid phase transitions. Spectral indicators are quantitatively correlated to the $I[\nu_a(CH_2)]/I[\nu_s(CH_2)]$, as this is the primary indicator of rotational and conformational order obtained empirically from Raman spectra. These indicators are interpreted in terms of alkane intramolecular motion, intermolecular interactions between alkyl chains, crystal structure of these solid materials, and the presence of methylene conformers. Results demonstrate that Raman spectroscopy is sensitive to very subtle changes in alkane chain structure and conformation. These results can be used to understand molecular interactions and structure−function relationships in alkane-based materials.

Introduction

Materials based on alkane-containing molecules are used in countless technological applications including self-assembled monolayers on metal and oxide surfaces (both two- and three-dimensional),[1−3] biological membranes,[4−6] biosensors,[7,8] Langmuir−Blodgett films,[9−14] chemically modified silicas for chromatography,[15−18] and polymeric alkane materials.[19−21] The desired attributes of alkane chain conformational order in these systems vary substantially from highly ordered (crystalline) to disordered (liquidlike) and are application-dependent. Alkane chain structure and interfacial properties dictate the function and utility of these materials. For example, biological membranes allow the transport of ions, proteins and other species from one side of the membrane to the other, as well as the lateral diffusion of membrane components within the bilayer. Thus, the alkane chains in the lipids of biological membranes must be partially liquidlike to allow this transport and lateral diffusion to occur. Alkane chains of a more rigid, crystalline character would restrict the transport of molecules across the membrane, while a membrane consisting of completely liquid alkane chains would lack the stability to remain intact.

In alkane-modified silicas used as stationary phase materials in chromatography, the conformational order of the alkane moieties governs the efficiency and selectivity of the separations.[22−25] Highly ordered, high-density stationary phase materials have been shown to have shape selectivity for planar polynuclear aromatic hydrocarbons, while less ordered stationary phase materials exhibit no geometric selectivity.[26] Clearly, describing alkane chain conformational order on the molecular level is crucial for understanding how such materials function in their respective applications.

Numerous experimental techniques have been used to study alkane-chain structure and conformation including nuclear magnetic resonance (NMR) spectroscopy,[20,26,27] Fourier transform-infrared spectroscopy (FTIR),[28−41] and Raman spectroscopy.[5,10,15−18,29,42−51] NMR experiments specifically probe alkane chain mobility, allowing information about conformational order to be inferred. Although a distinct correlation between chain mobility and conformational order exists, a direct measure of conformational order is necessary for understanding the subtleties of alkane structure and function. FTIR spectroscopy does offer direct conformational order information for alkane-based systems, an advantage over NMR spectroscopy. However, FTIR suffers from major limitations in spectral interference from solvents, resolution, activity of alkane vibrational modes, and experimental sensitivity and proves to be inadequate for studying subtle molecular changes in conformational order.[52]

In contrast, Raman spectroscopy has been shown to be a powerful experimental tool for determining subtle conformational changes in a wide variety of alkane-based systems.[5,15,16,49,52−55] Such conformational order information is useful in understanding the chemical environment of alkane chains and provides insight into the molecular interactions between alkane chains and their surroundings. Raman spectroscopy has the unique ability to provide direct information about conformational order, nondestructively and free from spectral interferences that plague FTIR spectroscopy.[28] In addition, the plethora of spectral bands in the ν(C−H), ν(C−C), and δ(C−H) regions of the Raman spectrum provide a great deal of information about conformational order including the extent of alkane chain coupling, intramolecular motion, relative numbers of gauche and trans conformers, and chain twisting and bending.[5,56]

Larsson and Rand first described the utility of Raman spectroscopy for determining alkane chain conformational order in lipids and lipid−protein complexes.[56] They noted that changes in spectral bands near 1100 cm^{-1} (later assigned to the $\nu(C-C)_G$ and $\nu(C-C)_T$ modes) correlate to relative numbers of gauche and trans conformers in alkane chains and that the intensity ratio of the 2885 cm^{-1} $\nu_a(CH_2)$ band to the 2850 cm^{-1} $\nu_s(CH_2)$ band, $I[\nu_a(CH_2)]/I[\nu_s(CH_2)]$, is a measure of lateral packing density of alkane chains and is itself an indication of order. Upon examining the relationship between $I[\nu_a(CH_2)]$/

* To whom correspondence should be addressed: (520) 621-8245, pembertn@u.arizona.edu.

† Current address: Department of Chemistry, Missouri Western State College, St. Joseph, MO 64507.

10.1021/jp014311n CCC: $22.00
Published on Web 07/09/2002

$I[\nu_s(CH_2)]$ and the intensity ratio of the $\nu(C-C)_G$ to the $\nu(C-C)_T$ modes near 1100 cm^{-1}, $I[\nu(C-C)_G]/I[\nu(C-C)_T]$, they concluded that the former is more sensitive than the latter to subtle changes in order for both disordered molecules and for molecules in an all-trans configuration.

It is important to note that the ratio $I[\nu_a(CH_2)]/I[\nu_s(CH_2)]$ measures different quantities for all-trans and disordered alkanes.[47] In the crystalline phase, the $I[\nu_a(CH_2)]/I[\nu_s(CH_2)]$ is a measure of rotational disorder in all-trans alkane chains, and in disordered, liquidlike alkanes, this ratio is additionally sensitive to the addition of gauche conformers. Thus, the $I[\nu_a(CH_2)]/I[\nu_s(CH_2)]$ is a subtle and sensitive indicator of order for crystalline alkane chains.

Larsson and Rand also noted an increase in intensity of the 2930 cm^{-1} $\nu_s(CH_3)_{FR}$ mode for increasingly disordered alkane assemblies. The intensity ratio of this mode to the 2850 cm^{-1} $\nu_s(CH_2)$ mode was later correlated to intermolecular coupling of alkane chains by Snyder et al.[47]

In addition to the work done by Larsson and Rand on lipid−protein complexes, Raman spectral indicators were also used extensively in the late 1960s and early 1970s to examine the conformational order of alkane chains in model systems including polymers and biological membranes.[5,46,47,54] More recently, these indicators have been used to describe the conformational order of more complex alkane assemblies similar to those mentioned above including self-assembled monolayers on a variety of substrates,[42,43,49,57] Langmuir−Blodgett layers,[10] and chemically modified silicas for reversed-phase liquid chromatography.[15−17] Even though discrete differences between bulk or solution phase alkane systems and the surface-bound systems exist, intermolecular hydrophobic interactions between alkane chains are similar. Therefore, the conformational order behavior of surface-confined alkane systems is complementary to that of bulk or solution phase materials when probed by Raman spectroscopy.

Despite the valuable work that has been done in an effort to understand the relationships between these Raman spectral indicators of conformational order, very little has been done to quantitatively correlate these indicators with the goal of understanding at what degree of disorder each parameter changes. In this report, the temperature-induced disordering of octadecane and a low molecular weight polyethylene allows quantitative correlation of numerous conformational order indicators in the $\nu(C-C)$, $\delta(C-H)$, and $\nu(C-H)$ spectral regions.

Experimental Section

Raman spectra were collected using 100 mW of p-polarized 532 nm radiation from a Coherent Verdi Nd:YVO_4 laser (Coherent, Inc., Santa Clara, CA) on a Spex Triplemate spectrograph. Slit settings were 0.5/7.0/0.150 mm for all experiments. A polarization scrambler was used just prior to the entrance slit to remove any effects of spectrometer polarization bias from the measured intensities. The detector in these experiments was a Princeton Instruments charged-coupled device (CCD) system based on a thinned, back-illuminated, antireflection coated RTE-110-PB CCD of pixel format 1100 × 330 that was cooled with liquid N_2 to −90 °C. Samples were sealed in 0.2 in diameter NMR tubes and positioned in the laser beam using a copper sample mount. The temperature of the copper mount was regulated by circulating 50:50 ethylene glycol:water through it and around the sample tube using a Neslab NTE-110 temperature controller, allowing temperature control from −15 to +110 °C. Temperatures greater than 110 °C were regulated by resistively heating the copper sample holder. Samples were allowed to equilibrate at each temperature for a minimum of 30 min prior to analysis. A minimum of three measurements were made at each temperature on samples independently prepared from the same batch of material. Integration times for each spectrum are provided in the figure captions. Low laser power and short acquisition times were used to avoid unnecessary sample heating by the laser beam.

Octadecane and low molecular weight polyethylene (average $M_w \sim 4000$; average $M_n \sim 1700$) were obtained from Aldrich and used as received.

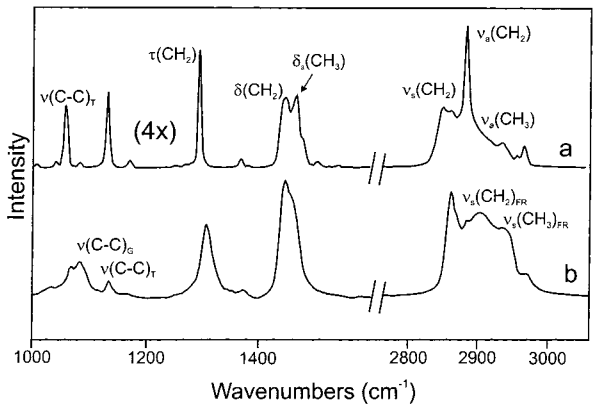

Figure 1. Raman spectra in the $\nu(C-C)$, $\delta(C-H)$ and $\nu(C-H)$ regions for octadecane at (a) 0 °C and (b) 60 °C. Integration time 2 min.

TABLE 1: Raman Peak Frequencies (cm^{-1}) and Assignments for Octadecane and Polyethylene

octadecane liquid	octadecane crystalline	polyethylene liquid	polyethylene cyrstalline	assignment[a]
1065	1062	1065	1062	$\nu(C-C)_T$
1081		1081		$\nu(C-C)_G$
1124	1128	1124	1128	$\nu(C-C)_T$
1303	1296	1302	1295	$\tau(CH_2)$
1369	1371	1369	1371	$\delta(CH_3)$
			1420	$\delta(CH_2)_{ORTHO}$
1440	1441	1440	1441	$\delta(CH_2)$
1450	1445	1450	1445	$\delta_a(CH_3)$
2852	2842	2852	2847	$\nu_s(CH_2)$
2888	2876	2886	2881	$\nu_a(CH_2)$
2925	2925	2925	2925	$\nu_s(CH_2)_{FR}$
2935	2935	2935	2935	$\nu_s(CH_3)_{FR}$
2965	2959	2965	2960	$\nu_a(CH_3)$

[a] ν = stretch; τ = twist; δ = bend and/or scissor.

Results and Discussion

General Overview of Alkane Conformational Order for Octadecane and Polyethylene from Raman Spectroscopy. Raman spectra of neat octadecane at 0 and 60 °C are shown in Figure 1 for two frequency regions, 1100−1600 and 2750−3050 cm^{-1}. The corresponding peak frequencies are reported in Table 1. Nine unique Raman spectral indicators for octadecane have been identified in the $\nu(C-H)$, $\delta(C-H)$, and $\nu(C-C)$ regions that reflect structural order in the alkane chain: the peak intensity ratios $I[\nu_a(CH_2)]/I[\nu_s(CH_2)]$, $I[\nu_s(CH_3)_{FR}]/I[\nu_s(CH_2)]$, and $I[\nu(C-C)_G]/I[\nu(C-C)_T]$; the integrated peak area ratio $A[\delta_a(CH_3)]/A[\delta(CH_2)]$; the peak frequencies of the $\nu_a(CH_2)$, $\nu_s(CH_2)$, and $\tau(CH_2)$ modes; the asymmetry of the $\tau(CH_2)$ mode; and the full-width-at-half-maximum (fwhm) of the $\tau(CH_2)$ mode. All of these are investigated here to elucidate the subtleties of alkane structure upon melting to provide a definitive molecular picture of this phenomenon. For

polyethylene, two spectral indicators in addition to those above result from the crystal field splitting of the $\delta(CH_2)$ in the crystalline state. These indicators are the are ratios $A[\delta_a(CH_3)]/\{A[\delta(CH_2)] + A[\delta(CH_2)_{ORTHO}]\}$ and the $A[\delta(CH_2)_{ORTHO}]/\{A[\delta_a(CH_3)] + A[\delta(CH_2)]\}$.

Although the ν(C−H) region (2750−3050 cm^{-1}) is complex for alkanes as a result of numerous spectral bands and Fermi resonance splittings, conformational order information can be obtained empirically from the peak intensity ratio $I[\nu_a(CH_2)]/I[\nu_s(CH_2)]$. This ratio spans a range from ∼0.6 to 2.0 for normal alkanes in the liquid (0.6−0.9) and crystalline (1.6−2.0) states.[52,55] This ratio is sensitive to subtle changes in conformational order from rotations, kinks, twists, and bends of the alkane chains; essentially, this ratio changes for any deviation from a perfect all-trans configuration.[46,56] Despite the extensive previous investigation and use of this intensity ratio as a measure of alkane order/disorder, no reports have appeared in which this ratio is quantitatively correlated to other chain coupling, twisting, bending, or gauche conformer spectral indicators of order.

Other spectral indicators of alkane order are also useful. The frequencies at which the $\nu_s(CH_2)$ and $\nu_a(CH_2)$ modes are observed reflect conformational order and interchain coupling; these modes are observed at ∼2853 and 2888 cm^{-1}, respectively, for octadecane in the liquid state, and decrease by 6−8 cm^{-1} in the crystalline state.[5,55] The frequency of the $\tau(CH_2)$ mode at ∼1300 cm^{-1} has also been related to the degree of coupling between alkane chains, with decoupling correlated with an increase in frequency of this mode. Chain coupling information can also be obtained from the intensity ratio of $\nu_s(CH_3)_{FR}$ at ∼2930 cm^{-1} to $\nu_s(CH_2)$ at ∼2850.[47] As the chains decouple (intermolecular interactions decrease), the terminal methyl groups experience increased rotational and vibrational freedom, and the intensity ratio of $\nu_s(CH_3)_{FR}$ to $\nu_s(CH_2)$ increases.

Conformational order information for alkanes can be obtained from vibrational modes in the ν(C−C) and δ(C−H) regions as well. The relative number of gauche and trans conformers in alkane chains is indicated by the intensity ratio of $\nu(C-C)_G$ (∼1080 cm^{-1}) to $\nu(C-C)_T$ (∼1062 cm^{-1}). For octadecane, this intensity ratio spans a range from zero in the crystalline state to 1.1−1.3 in the liquid state. Unlike modes in the ν(C−H) region, the ν(C−C) modes are only sensitive to true gauche and trans conformations and not to methylene rotations or other bond deformations.[56]

Two other spectral envelopes of bands contain conformational order information, those centered around 1300 and 1450 cm^{-1}. The $\tau(CH_2)$ (∼1300 cm^{-1}) is superimposed on a number of modes including, but not limited to, the methylene wag, the H−C−H deformation, and other methylene deformation modes.[52] The intensities of these modes change from liquid to crystalline states of alkanes and are primarily sensitive to conformer changes between gauche and trans. The intensity changes of the underlying modes cause visible changes in the $\tau(CH_2)$ and can be quantified by changes in width, asymmetry, and frequency of this mode.

The spectral region near 1450 cm^{-1} contains a number of overlapping deformation modes but is dominated by the methylene scissor mode ($\delta(CH_2)$ at ∼1440 cm^{-1}) and the antisymmetric methyl bend ($\delta_a(CH_3)$ at ∼1460 cm^{-1}).[52,58] An increase in the integrated peak area ratio of these two envelopes, designated as $A[\delta_a(CH_3)]/A[\delta(CH_2)]$, is an indication of the increased population of methyl and methylene groups free to undergo the scissor or bending motion, respectively. Structurally, this denotes increased methyl and methylene intramolecular motion that increases with alkane chain decoupling.

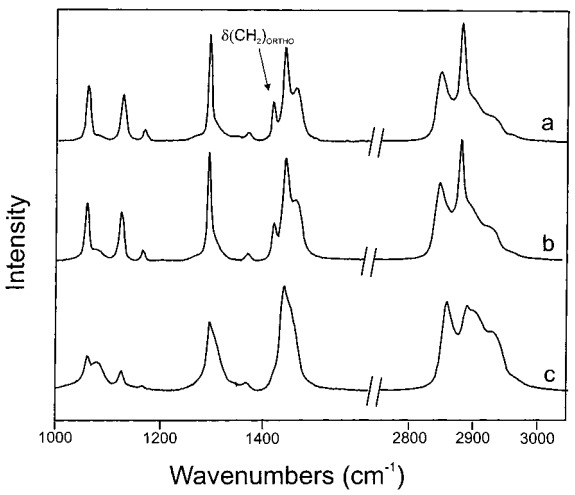

Figure 2. Raman spectra in the ν(C−C), δ(C−H) and ν(C−H) regions for polyethylene at (a) 0 °C, (b) 74 °C, and (c) 100 °C. Integration time 2 min.

The phase transition for neat octadecane (melting point 29 °C) is abrupt and occurs over an ∼1 °C range, typical for small molecules. As a result, the conformational order information obtained near the phase transition is limited by a combination of the kinetics of the transition and the temperature resolution (≥0.5 °C) of the experimental system. Due to the difficulty in controlling the melting event at the phase transition, spectra obtained during the phase transition reflect those for a biphasic mixture; thus, the spectral response represents the average conformational state of liquid and solid phases present in the biphasic mixture.

To facilitate a greater understanding of more subtle changes in conformational order throughout the phase transition, a low molecular weight polyethylene (melting point ∼98 °C) is studied here as well. The phase transition for polyethylene is more gradual, and conformational order is observed to change over a temperature range of several degrees. Raman spectra of polyethylene from 0 to 100 °C are shown for the ν(C−C), δ(C−H) and ν(C−H) regions in Figure 2 with the corresponding peak frequencies in Table 1.

Comparing these spectral data to those of octadecane, the most obvious difference is the presence of the $\delta(CH_2)_{ORTHO}$ mode at ∼1420 cm^{-1} and the loss of intensity of the $\delta(CH_2)$ mode at 1440 cm^{-1} at low temperatures. The $\delta(CH_2)_{ORTHO}$ mode signifies an orthorhombic crystal structure of polyethylene and results from crystal field splitting of the $\delta(CH_2)$ mode at 1440 cm^{-1}.[59] The intensity of the $\delta(CH_2)_{ORTHO}$ decreases with increasing temperature as the volume unit cell of the crystal expands and finally disappears in the liquid phase. As a result of this crystal field splitting, quantification of the peaks in this region for polyethylene from curve fitting are presented as the sum of the integrated peak areas of the $\delta(CH_2)$ and $\delta(CH_2)_{ORTHO}$ bands.[60]

Raman Spectroscopy of Octadecane. The correlation between $I[\nu_a(CH_2)]/I[\nu_s(CH_2)]$ and $I[\nu(C-C)_G]/I[\nu(C-C)_T]$ is shown in Figure 3. The plot is divided into liquid, biphasic, and crystalline regions by dashed lines. As noted above, the difficulty in temperature control in the phase transition region renders these lines only an approximation of the phase boundary; thus, they are intended only as a guide to the reader. The crystalline region spans a temperature range from −15 to +28 °C, the biphasic region is at a temperature of ∼29 °C, and the liquid region is between 30 and 100 °C.

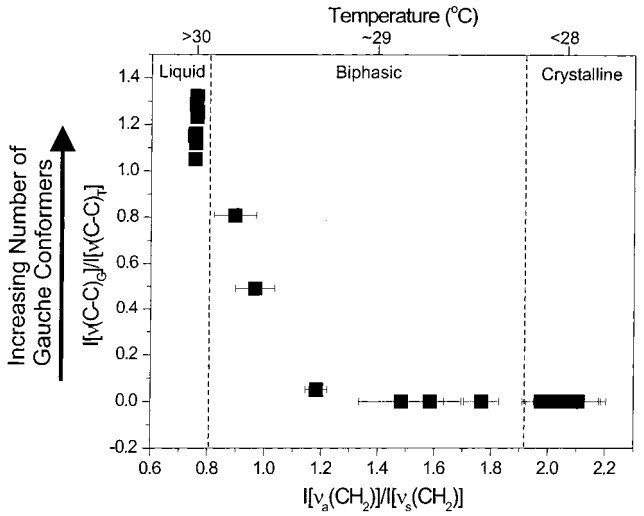

Figure 3. Intensity ratio of $\nu(C-C)_G$ to $\nu(C-C)_T$ as a function of the intensity ratio of $\nu_a(CH_2)$ to $\nu_s(CH_2)$ for octadecane. Error bars are included for each point but may be smaller than the size of the points.

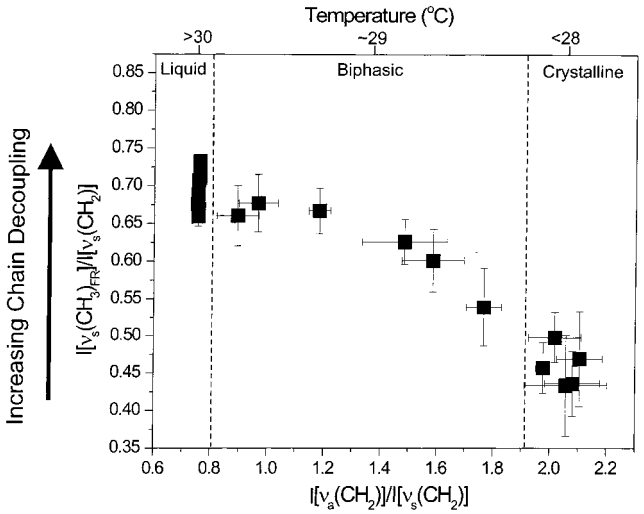

Figure 4. Intensity ratio of $\nu_s(CH_3)_{FR}$ to $\nu_s(CH_2)$ as a function of the intensity ratio of $\nu_a(CH_2)$ to $\nu_s(CH_2)$ for octadecane.

In the crystalline state, no gauche conformers exist in alkanes; however, some aspect of conformational order changes with increasing temperature, as indicated by a decrease in $I[\nu_a(CH_2)]/I[\nu_s(CH_2)]$ from 2.1 to 1.5. These changes are thought to be due to methyl and methylene rotational disorder, predominantly near the ends of the alkane chains. Further into the biphasic region, the average number of gauche conformers increases, starting at a value of $I[\nu_a(CH_2)]/I[\nu_s(CH_2)]$ of ~1.2 and continuing for decreasing values of $I[\nu_a(CH_2)]/I[\nu_s(CH_2)]$ to 0.75. In the liquid phase, the extent of deviation from the all-trans state remains constant (i.e., $I[\nu_a(CH_2)]/I[\nu_s(CH_2)]$ is constant), while the relative number of gauche conformers increases with increasing thermal energy. In this region, the rotational disorder responsible for the variance of $I[\nu_a(CH_2)]/I[\nu_s(CH_2)]$ in the biphasic region is converted to true gauche conformers with increasing temperature.

Alkane intermolecular interactions, specifically interchain coupling, for octadecane as embodied in $I[\nu_s(CH_3)_{FR}]/I[\nu_s(CH_2)]$ is correlated to $I[\nu_a(CH_2)]/I[\nu_s(CH_2)]$ in Figure 4. Alkane chain coupling decreases with increasing rotational disorder ($I[\nu_a(CH_2)]/I[\nu_s(CH_2)]$ decreases from 2.1 to 1.3). Here alkane chains spread out sufficiently that rotational disorder becomes extensive. At temperatures in the vicinity of the melting

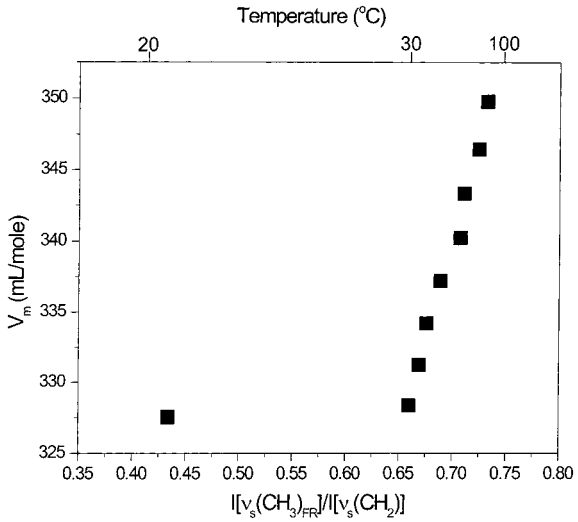

Figure 5. Molar volume (milliliters/mole) of octadecane as a function of the intensity ratio of $\nu_s(CH_3)_{FR}$ to $\nu_s(CH_2)$.

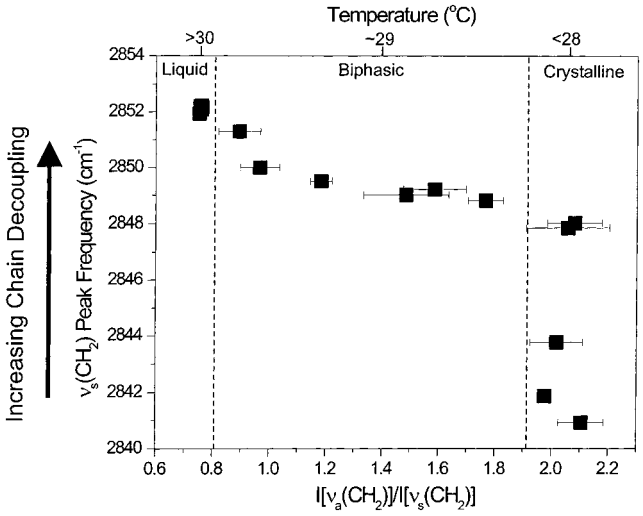

Figure 6. $\nu_s(CH_2)$ peak frequency as a function of the intensity ratio of $\nu_a(CH_2)$ to $\nu_s(CH_2)$ for octadecane.

temperature where $I[\nu_a(CH_2)]/I[\nu_s(CH_2)]$ attains values of 1.2−0.8, the chains are sufficiently decoupled to allow gauche conformers to be formed. Decoupling continues in the liquid state with increased thermal energy, although the rotational disorder is at its maximum, and hence, the $I[\nu_a(CH_2)]/I[\nu_s(CH_2)]$ remains constant. These changes are consistent with a change in molar volume of the liquid alkane as a function of increasing temperature. That such a change is indeed occurring can be seen from the plot in Figure 5 of the molar volume for ocatdecane in the liquid state[60] as a function of the spectral indicator for interchain decoupling, $I[\nu_s(CH_3)_{FR}]/I[\nu_s(CH_2)]$. In this plot, the molar volume increases only slightly over the solid/liquid phase boundary, but then increases dramatically in the liquid phase.

Alkane chain coupling information can also be obtained from the peak frequency of $\nu_s(CH_2)$; this parameter is correlated to $I[\nu_a(CH_2)]/I[\nu_s(CH_2)]$ in Figure 6. The $\nu_a(CH_2)$ and $\tau(CH_2)$ peak frequencies are also indicators of interchain coupling and are correlated to $I[\nu_a(CH_2)]/I[\nu_s(CH_2)]$ in Figures 1S and 2S in the Supporting Information. Although the $\nu(CH_2)$ peak frequencies and $I[\nu_s(CH_3)_{FR}]/I[\nu_s(CH_2)]$ are indicators of interchain coupling, it is important to note that they represent measures of different parameters. The peak frequencies are sensitive to subtle chain interactions that may dampen or otherwise affect $\nu(CH_2)$ vibrations. In contrast, the $I[\nu_s(CH_3)_{FR}]/I[\nu_s(CH_2)]$ is sensitive

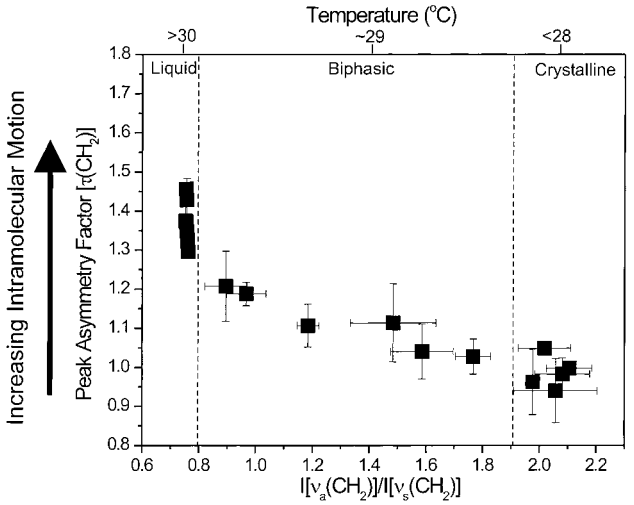

Figure 7. $\tau(CH_2)$ peak asymmetry factor as a function of the intensity ratio of $\nu_a(CH_2)$ to $\nu_s(CH_2)$ for octadecane

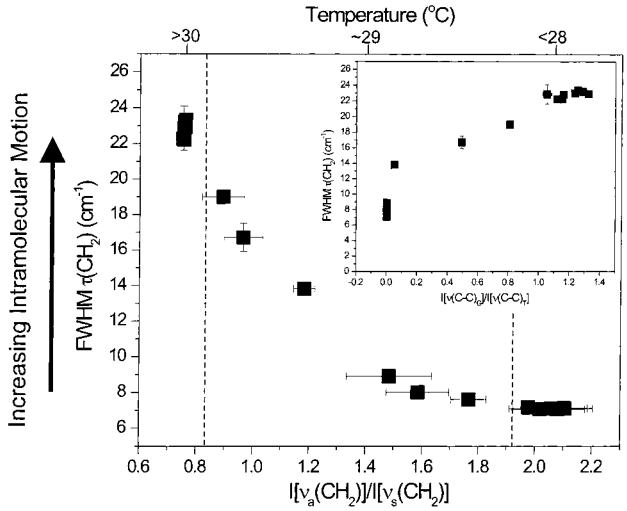

Figure 8. $\tau(CH_2)$ full-width half-maximum (fwhm) as a function of the intensity ratio of $\nu_a(CH_2)$ to $\nu_s(CH_2)$ for octadecane. Inset: $\tau(CH_2)$ fwhm as a function of the intensity ratio of $\nu(C-C)_G$ to $\nu(C-C)_T$ for octadecane.

to larger coupling interactions that affect the terminal methyl group of the alkane chains and molar volume changes of the material. The $\nu(CH_2)$ vibrations are damped by highly coupled alkane chains in the crystalline material and are shifted to lower frequency. As the thermal energy of the system increases in the solid, the chains decouple slightly and the frequencies increase. Through the phase transition, the peak frequencies increase slightly and the chains further decouple.

The $\nu_s(CH_2)$ peak frequency is a popular indicator of order not only in bulk alkane systems but also in surface-bound alkane systems as probed by surface vibrational methods such as surface FTIR and vibrational sum-frequency generation.[28−41,61] This indicator should be used with some caution, however, in light of the fact that the $\nu_s(CH_2)$ frequency shifts by 6−8 cm^{-1} for neat octadecane in the crystalline state. This shift is a clear indication that this indicator alone does not adequately describe the conformational state of these systems. While the lowest frequency of this mode is indeed an indication of a highly ordered crystalline state, and the frequency of $\nu_s(CH_2)$ is sensitive to chain decoupling in the crystal, information regarding the disorder imparted to the alkane chains during a phase transition and in the liquid phase is not available from this parameter.

Alkane chain intramolecular motion and chain coupling as indicated by the $\tau(CH_2)$ peak asymmetry and width (fwhm) are correlated with $I[\nu_a(CH_2)]/I[\nu_s(CH_2)]$ in Figures 7 and 8, respectively. The peak asymmetry is quantified by calculating an asymmetry factor equal to the ratio of the frequency distance from the right and left edges (measured at the fwhm) to the peak frequency. As shown in Figure 7, the $\tau(CH_2)$ remains symmetric (asymmetry factor = 1.0) for $I[\nu_a(CH_2)]/I[\nu_s(CH_2)]$ values between 2.1 and 1.5. In the melting region, the peak becomes slightly asymmetric as the rotational order decreases ($I[\nu_a(CH_2)]/I[\nu_s(CH_2)]$ values between 1.2 and 0.8). Once in the liquid state, this peak continues to increase in asymmetry as the rotational disorder remains at its maximum. Temperature regions in which the $\tau(CH_2)$ peak becomes asymmetric coincide with regions in which the number of gauche conformers increases, as indicated by the $I[\nu(C-C)_G]/I[\nu(C-C)_T]$. A similar trend is observed for the increase in the fwhm of the $\tau(CH_2)$ mode with both increasing rotational disorder and with increasing gauche conformers, as shown in the inset of Figure 8. Clearly the development of asymmetry in this band results from changes in the population of gauche conformers. The fact that a discrete band is not observed for the $\tau(CH_2)$ mode of gauche conformers suggests that a range of alkane chain twisting motions are accessible to gauche conformers whereas a much narrower range is accessible to trans conformers. In light of the considerable increased rotational disorder that accompanies the formation of gauche conformers, this observation is not surprising.

Similar behavior is observed for the correlation between the $A[\delta_a(CH_3)]/A[\delta(CH_2)]$ and $I[\nu_a(CH_2)]/I[\nu_s(CH_2)]$, as shown in Figure 3S in the Supporting Information. The complexity and general uncertainty of the peak assignments in this region lead to the use of integrated peak area ratios instead of peak intensity ratios as used for the other indicators. The peak areas of these two modes were determined using a Gaussian line shape analysis of the spectra. These fits are also shown in Figure 3S in the Supporting Information. The $A[\delta_a(CH_3)]/A[\delta(CH_2)]$ remains constant until gauche conformers are introduced into the alkane structure. This value increases in the biphasic region and continues to increases with increased thermal energy in the liquid state. This trend is again a result of the increasing population of gauche conformers and the increased intramolecular motion allowed as octadecane melts.

Raman Spectroscopy of Polyethylene. The rapidity of the phase transition for octadecane makes acquisition of quality spectroscopic information near the phase transition difficult. Moreover, the phase transition for octadecane results in a biphasic mixture of species and not a system containing systematically varying disorder. For these reasons, the Raman spectral response for polyethylene is also probed on both sides of the phase transition. In light of its fewer degrees of freedom and a less abrupt phase transition, this system provides a more appropriate model for surface-confined alkane systems. For this investigation, a medium density ($\rho \sim 0.92$ g/cm^3), linear polyethylene is used to spectroscopically examine alkane melting. Due to differences in the thermal behavior of this system as compared to octadecane, the polyethylene data are presented in a slightly different format in that an expanded temperature range is considered and the three regions identified are the termed the crystalline, amorphous solid, and liquid regions.

The correlation between $I[\nu(C-C)_G]/I[\nu(C-C)_T]$ and $I[\nu_a(CH_2)]/I[\nu_s(CH_2)]$ for polyethylene is shown in Figure 9. The behavior for polyetheylene is similar to that observed for

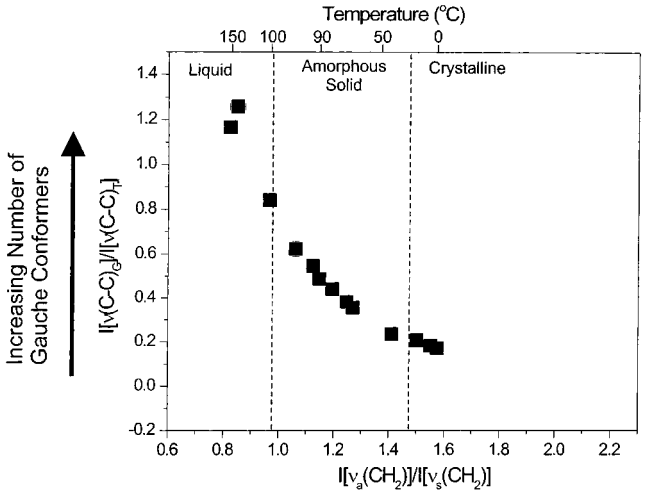

Figure 9. Intensity ratio of $\nu(C-C)_G$ to $\nu(C-C)_T$ as a function of the intensity ratio of $\nu_a(CH_2)$ to $\nu_s(CH_2)$ for polyethylene.

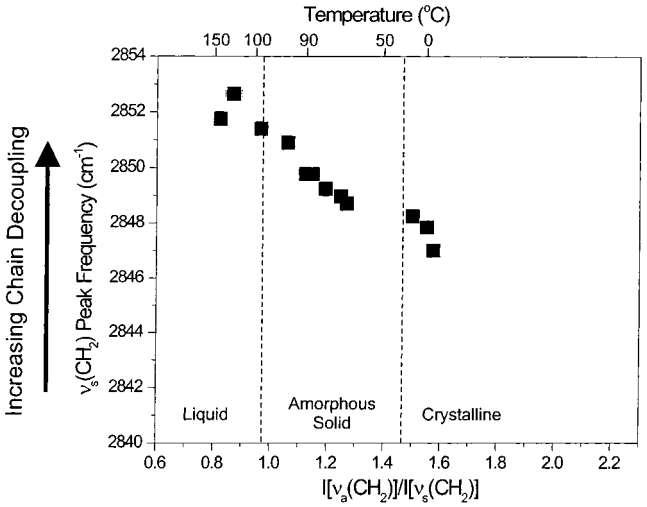

Figure 10. $\nu_s(CH_2)$ peak frequency as a function of the intensity ratio of $\nu_a(CH_2)$ to $\nu_s(CH_2)$ for polyethylene.

octadecane (Figure 3) at high temperatures in that the number of gauche conformers increases significantly between $I[\nu_a(CH_2)]/I[\nu_s(CH_2)]$ values of 1.2 and 0.8 and continues to increase in the liquid phase while $I[\nu_a(CH_2)]/I[\nu_s(CH_2)]$ remains constant. The most significant differences in order behavior between the two materials occur in the low-temperature region. Polyethylene is not as inherently ordered as octadecane at these temperatures due to a small number of gauche defects in the polymer chains that still exist even when $I[\nu_a(CH_2)]/I[\nu_s(CH_2)]$ has values of 1.6−1.3. This inherent disorder is due to the orthorhombic crystal structure of the polymer (in contrast to the hexagonal crystal structure of octadecane) in which the polymer chains contain hairpin bends.[19,62,63] The more restrictive orthorhombic crystal structure of the polyethylene results in fewer degrees of freedom for the chains to undergo decoupling and rotational disorder.

Insight into the extent of interchain coupling through the $\nu_s(CH_2)$ peak frequency is correlated with $I[\nu_a(CH_2)]/I[\nu_s(CH_2)]$ in Figure 10. In solid polyethylene, the $\nu_s(CH_2)$ peak frequency never gets as low as it does for solid octadecane, indicating an inherently more decoupled crystalline system. During melting, this peak frequency increases with increasing temperature in the solid as the orthorhombic unit cell expands and the chains decouple. Beyond the melting temperature, the frequency continues to increase in the liquid phase as the thermal energy

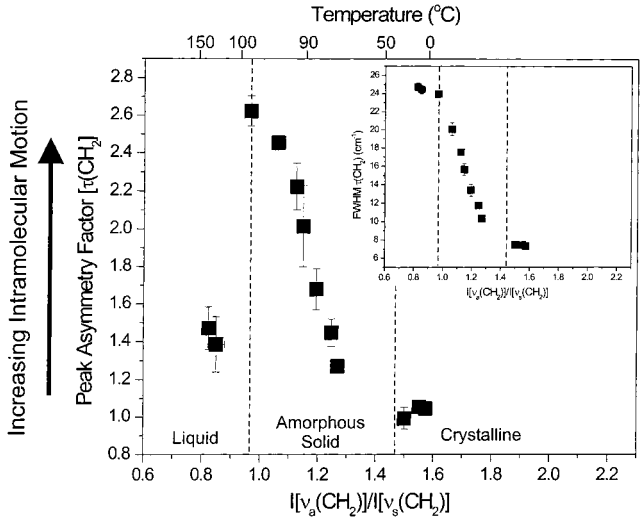

Figure 11. $\tau(CH_2)$ peak asymmetry factor as a function of the intensity ratio of $\nu_a(CH_2)$ to $\nu_s(CH_2)$ for polyethylene. Inset: $\tau(CH_2)$ fwhm as a function of the intensity ratio of $\nu_a(CH_2)$ to $\nu_s(CH_2)$ for polyethylene.

of the system increases and chain decoupling increases, similar to the behavior observed for octadecane.

The correlations of the $\nu_a(CH_2)$ and $\tau(CH_2)$ peak frequencies and the $I[\nu_s(CH_3)_{FR}]/I[\nu_s(CH_2)]$ with $I[\nu_a(CH_2)]/I[\nu_s(CH_2)]$ are shown in Figures 4S and 5S in the Supporting Information. $I[\nu_s(CH_3)_{FR}]/I[\nu_s(CH_2)]$ correlates similarly with $I[\nu_a(CH_2)]/I[\nu_s(CH_2)]$ for polyethylene as for octadecane: increased chain decoupling (indicated by an increase in $I[\nu_s(CH_3)_{FR}]/I[\nu_s(CH_2)]$) occurs with increasing disorder. Polyethylene chain decoupling can also be correlated to an increase in specific volume (milliliters/gram) in the solid and liquid forms of the polymer as described for a similar polyethylene by Sibukawa et al.[64] For polyethylenes of similar physical characteristics, the specific volume increases slightly (<10%) in going from the crystalline to the amorphous solid state (20 °C to the melting point) and then increases ∼25% for increasing temperatures throughout the liquid phase. These observations are similar to those made for the molar volume changes in octadecane (Figure 5), although the differences in magnitude of the changes in molar and specific volumes for octadecane and polyethylene, respectively, stem from the unique physical and structural properties of these two systems.

As shown by the data in Figure 11, the correlation of the $\tau(CH_2)$ peak asymmetry and the $\tau(CH_2)$ fwhm (inset) with the $I[\nu_a(CH_2)]/I[\nu_s(CH_2)]$ provides insight into intramolecular motion of the alkane chains. In contrast to octadecane, the $\tau(CH_2)$ mode for polyethylene becomes extremely asymmetric at higher temperatures, reaching a distinct *maximum* value of asymmetry at the melting point. Interestingly, at temperatures above the solid/liquid-phase transition, the $\tau(CH_2)$ peak asymmetry decreases sharply and becomes comparable in value to that for liquid octadecane. Other researchers reported similar qualitative observations of this increasing asymmetry of the $\tau(CH_2)$ mode for polyethylene and attributed it to an increase in population of amorphous states of the polymer.[48,51] For octadecane, the amorphous component (i.e., the liquid phase) is only present at temperatures above the transition temperature. No amorphous solid exists for solid octadecane. Conversely, for polyethylene, an amorphous component develops in the solid material as temperature increases but stays below the transition temperature. The increase in the $\tau(CH_2)$ peak asymmetry is a quantitative measure of this amorphous character of solid polyethylene, since

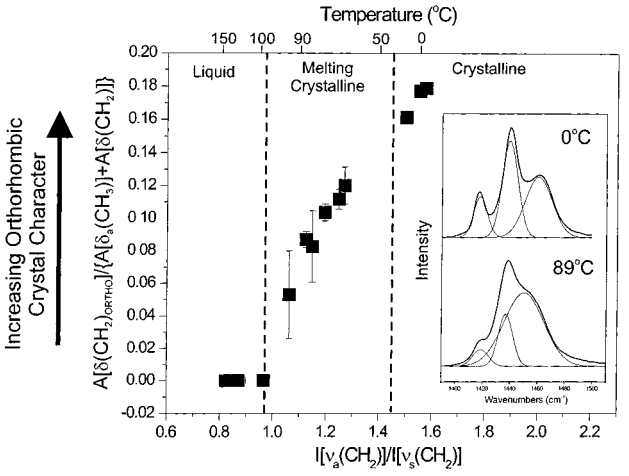

Figure 12. Peak area ratio of $\delta(CH_2)_{ORTHO}$ to $[\delta_a(CH_3) + \delta(CH_2)]$ as a function of the intensity ratio of $\nu_a(CH_2)$ to $\nu_s(CH_2)$ for polyethylene. Inset: Raman spectra of the deformation modes (1390−1510 cm^{-1}) peak fit using a Gaussian distribution at 0 and 89 °C.

this vibration is sensitive to changes in the crystalline, amorphous solid, and amorphous liquid phases.

The $\tau(CH_2)$ fwhm increases with decreasing conformational order and increases with the number of gauche conformers, as shown in the inset of Figure 11. This behavior is similar to that observed for octadecane. While the asymmetry of the $\tau(CH_2)$ is dependent on rotational disorder, the population of gauche conformers, and the crystallinity of the material (crystalline, amorphous solid, or liquid), the $\tau(CH_2)$ fwhm depends only on the population of gauche conformers and rotational disorder.

Similar behavior occurs for the $A[\delta_a(CH_3)]/\{A[\delta(CH_2)] + A[\delta(CH_2)_{ORTHO}]\}$ when correlated to the $I[\nu_a(CH_2)]/I[\nu_s(CH_2)]$ for polyethylene as shown in Figure 6S in the Supporting Information. In this case, $A[\delta_a(CH_3)]/\{A[\delta(CH_2)] + A[\delta(CH_2)_{ORTHO}]\}$ increases with the number of gauche conformers, indicating increased intramolecular motion of the alkane chains. This behavior is similar to that observed for octadecane throughout the biphasic region.

The degree of orthorhombic crystalline character of the polyetheylene can be determined by monitoring changes in peak area of the $\delta(CH_2)_{ORTHO}$ as a function of temperature. In quantifying a change in crystallinity, it is important to account for the total area of this deformation mode, since it comes from the crystal field splitting of $\delta(CH_2)$ (1440 cm^{-1}). Therefore, the area of $\delta(CH_2)_{ORTHO}$ normalized to the summed areas of the $\delta_a(CH_3)$ and $\delta(CH_2)$ modes is correlated to $I[\nu_a(CH_2)]/I[\nu_s(CH_2)]$ in Figure 12 using an area ratio similar to that described by Abbate et al.[60] The crystalline polymer loses its orthorhombic character with increasing temperature as the unit cell expands. Once the polymer undergoes the solid/liquid-phase transition, the $\delta(CH_2)_{ORTHO}$ mode disappears completely.

Comparison of Common Raman and IR−Active Indicators of Conformational Order. Conformational order is not as easily assessed from infrared spectroscopy due to limited resolution, inactivity, and weakness of major alkane vibrational modes, and poor experimental sensitivity when compared to the results presented here for Raman spectroscopy. Nonetheless, the IR spectra of alkanes also contain modes that are sensitive to alkane conformational order. Specifically, those modes cited most frequently as containing information about conformational order include the $\nu_s(CH_2)$ and $\nu_a(CH_2)$ peak frequencies (∼2850 and ∼2922 cm^{-1}) and the ν(C−C) gauche, trans, and kink modes (∼1000−1300 and ∼620−700 cm^{-1}).[28−40] These indicators are important in elucidating alkane structure in materials; however, the chain coupling information and numbers of gauche and trans conformers provided by these indicators are only a small portion of the information necessary for a complete molecular understanding of the disorder in these materials. More direct comparison between Raman and IR spectral data for elucidation of conformational order is difficult, because the majority of intense Raman-active modes are either weak in the IR or IR-inactive and vice versa.[52] Thus, the completeness of the conformational order indicators provided by the Raman spectra provide a compelling case for the better utility of Raman spectroscopy relative to infrared spectroscopy for the determination of conformational order in alkane-based systems whenever possible.

Summary

The work described here demonstrates the utility of Raman spectroscopy in determining the general conformational order, specifically subtle changes in intermolecular interactions, intramolecular motion, and chain conformations, for alkane-based systems. For octadecane, thermally induced alkane disordering is initiated by decoupling of the alkane chains with concomitant rotational disorder in the hexagonal crystal as indicated by increasing values of $I[\nu_s(CH_3)_{FR}]/I[\nu_s(CH_2)]$ (0.4 to 0.65) and $\nu_s(CH_2)$ peak frequency (2841 to 2849 cm^{-1}) and decreasing values of $I[\nu_a(CH_2)]/I[\nu_s(CH_2)]$ (2.1 to 1.4). Chain decoupling is accompanied by an increase in intramolecular motion, as indicated by an increase in the values of $A[\delta_a(CH_3)]/A[\delta(CH_2)]$ (0.8 to 4.9), the $\tau(CH_2)$ fwhm (7 to 19 cm^{-1}), and the $\tau(CH_2)$ peak frequency (1295 to 1300 cm^{-1}). Once adequate thermal energy has been added to the system to sufficiently decouple the alkane chains, gauche conformers form and the increase in decoupling ceases while the octadecane becomes more liquid-like. The increase in gauche conformers is indicated by the increase in the value of $I[\nu(C-C)_G]/I[\nu(C-C)_T]$ (0 to 0.8) while the $I[\nu_s(CH_3)_{FR}]/I[\nu_s(CH_2)]$ (∼0.65) and the $\nu_s(CH_2)$ peak frequency (∼2849 cm^{-1}) remain constant. Once the phase transition from crystalline to liquid is complete, significant increases in the molar volume of the liquid occur with increased temperature due to the conversion of methylene trans and partially rotated conformers to true gauche conformers. These changes are reflected as increases in $I[\nu_s(CH_3)_{FR}]/I[\nu_s(CH_2)]$ (0.65 to 0.75), the $\nu_s(CH_2)$ peak frequency (2849 to 2852 cm^{-1}), and $I[\nu(C-C)_G]/I[\nu(C-C)_T]$ (0.8 to 1.3), while the value of $I[\nu_a(CH_2)]/I[\nu_s(CH_2)]$ (∼0.75) remains constant.

Similar behavior occurs in the thermally induced disordering of polyethylene, with the exception of the unique structural differences between the hexagonal crystal structure of octadecane and the orthorhombic structure of crystalline polyethylene, indicated by the presence of the $\delta(CH_2)_{ORTHO}$ mode and the highly asymmetric $\tau(CH_2)$ mode of melting crystalline polyethylene. At temperatures below the melting temperature, the onset of alkane chain disordering stems from decoupling of the chains and increased rotational motion of the chains in the orthorhombic crystal as indicated by an increase in the values of $I[\nu_s(CH_3)_{FR}]/I[\nu_s(CH_2)]$ (0.4 to 0.65) and the $\nu_s(CH_2)$ peak frequency (2846 to 2850 cm^{-1}), a decrease in the value of $I[\nu_a(CH_2)]/I[\nu_s(CH_2)]$ (1.6 to 1.1), and the presence of the $\delta(CH_2)_{ORTHO}$ mode (1420 cm^{-1}). Increased chain decoupling is accompanied by an increase in intramolecular motion, as indicated by an increase in the values of $A[\delta_a(CH_3)]/A[\delta(CH_2) + \delta(CH_2)_{ORTHO}]$ (0.8 to 4.5), the $\tau(CH_2)$ fwhm (7 to 19 cm^{-1}), and the $\tau(CH_2)$ peak frequency (1295 to 1300 cm^{-1}). Once adequate thermal energy has been added to the system to sufficiently decouple the alkane chains, additional gauche

conformers form, and the increase in decoupling ceases. In contradistinction to octadecane, these changes begin while polyethylene is still in the solid-state and function to add more amorphous character to the solid prior to true melting. The increase in gauche conformers is indicated by the increase in the value of $I[\nu(C-C)_G]/I[\nu(C-C)_T]$ (0.2 to 0.8) while the $I[\nu_s(CH_3)_{FR}]/I[\nu_s(CH_2)]$ ($\sim$0.65) and the $\nu_s(CH_2)$ peak frequency ($\sim$2851 cm^{-1}) remain constant. Once the phase transition from crystalline to liquid is complete, significant increases in the molar volume of the liquid occur with increased temperature due to the conversion of methylene trans and partially rotated conformers to true gauche conformers. These changes are reflected as increases in $I[\nu_s(CH_3)_{FR}]/I[\nu_s(CH_2)]$ (0.65 to 0.75), the $\nu_s(CH_2)$ peak frequency (2851 to 2853 cm^{-1}), and $I[\nu(C-C)_G]/I[\nu(C-C)_T]$ (0.8 to 1.3), while the value of $I[\nu_a(CH_2)]/I[\nu_s(CH_2)]$ ($\sim$0.75) remains constant. In addition, the conversion of the orthorhombic cystal to an amorphous solid, and finally, to the amorphous liquid is indicated by an increase in $\tau(CH_2)$ peak asymmetry (1.0 to 2.6) and a decrease in $A[\delta(CH_2)_{ORTHO}]/[A[\delta(CH_2)] + A[\delta(CH_2) + \delta(CH_3)]]$ (0.18 to 0.)

Acknowledgment. We gratefully acknowledge support of this research by the Department of Energy, Office of Basic Energy Science (DE-FG03-95ER14546).

Supporting Information Available: Correlation plots of additional but less important Raman spectral indicators of alkane conformational order are available. This material is available free of charge via the Internet at http://pubs.acs.org.

References and Notes

(1) Templeton, A. C.; Wuelfing, W. P.; Murray, R. W. *Acc. Chem. Res.* **2000**, *33*, 27.
(2) Ulman, A. *An Introduction to Ultrathin Organic Films from Langmuir−Blodgett to Self-Assembly*; Academic Press: San Diego, 1991.
(3) Ulman, A. *Chem. Rev.* **1996**, *96*, 1533.
(4) Yellin, N.; Levin, I. W. *Biochim. Biophys. Acta* **1977**, *489*, 177.
(5) Gaber, B. P.; Peticolas, W. L. *Biochim. Biophys. Acta* **1977**, *465*, 260.
(6) Erwin, J. A. *Lipid and Biomembranes of Eukaryotic Microorganisms*; Academic Press: New York, 1973.
(7) Haupt, K.; Mosbach, K. *Chem. Rev.* **2000**, *100*, 2495.
(8) Crooks, R. M.; Ricco, A. J. *Acc. Chem. Res.* **1998**, *31*, 219.
(9) Mendelsohn, R.; Moore, D. J. *Chem. Phys. Lipids* **1998**, *96*, 141.
(10) Muniz-Miranda, M.; Puggelli, M.; Ricceri, R.; Gabrielli, G. *Langmuir* **1996**, *12*, 4417.
(11) Roberts, G. *Langmuir−Blodgett Films*; Plenum Press: New York, 1990.
(12) Selle, C.; Pohle, W.; Fritzsche, H. *J. Mol. Struct.* **1999**, *480−481*, 401.
(13) Silvestro, L.; Axelsen, P. H. *Chem. Phys. Lipids* **1998**, *96*, 69.
(14) Lewis, R. N. A. H.; McElhaney, R. N. *Chem. Phys. Lipids* **1998**, *96*, 9.
(15) Ho, M.; Cai, M.; Pemberton, J. E. *Anal. Chem.* **1997**, *69*, 2613.
(16) Ho, M.; Pemberton, J. E. *Anal. Chem.* **1998**, *70*, 4915.
(17) Pemberton, J. E.; Ho, M.; Orendorff, C. J.; Ducey, M. W. *J. Chromatogr. A* **2001**, *913*, 243.
(18) Ducey, M. W.; Orendorff, C. J.; Sander, L. C.; Pemberton, J. E. *Anal. Chem.*, submitted for publication.
(19) Boenig, H. V. *Polyolefins: Structure and Properties*; Elsevier Publishing Co.: Amsterdam, 1966.
(20) Clauss, J.; Schmidt-Rohr, K.; Adam, A.; Boeffel, C.; Spiess, H. W. *Macromolecules* **1992**, *25*, 5208.
(21) O'Brien, D. F.; Armitage, B.; Benedicto, A.; D. E. Bennett; Lamparski, H. G.; Lee, Y.; Srisiri, W.; Sisson, T. M. *Acc. Chem. Res.* **1998**, *31*, 861.
(22) Dorsey, J. G.; Dill, K. A. *Chem. Rev.* **1989**, *89*, 331.
(23) Dorsey, J. G.; Cooper, W. T. *Anal. Chem.* **1994**, *66*, 857A.
(24) Tchapla, A.; Heron, S.; Lesellier, E. *J. Chromatogr. A* **1993**, *656*, 81.
(25) Schunk, T. C.; Burke, M. F. *J. Chromatogr. A* **1993**, *656*, 289.
(26) Ellwanger, A.; Sander, L. C.; Bell, C. M.; Handel, H.; Albert, K. *Solid State Nucl. Magn. Reson.* **1997**, *9*, 191.
(27) Pursch, M.; Brindle, R.; Ellwanger, A.; Sander, L. C.; Bell, C. M.; Handel, H.; Albert, K. *Solid State Nucl. Magn. Reson.* **1997**, *9*, 191.
(28) Sander, L. C.; Callis, J. B.; Field, L. R. *Anal. Chem.* **1983**, *55*, 1068.
(29) Snyder, R. G.; Maroncelli, M.; Qi, S. P.; Strauss, H. L. *Science* **1981**, *214*, 188.
(30) Hostetler, M. J.; Stokes, J. J.; Murray, R. W. *Langmuir* **1996**, *12*, 3604.
(31) Gericke, A.; Mendelsohn, R. *Langmuir* **1996**, *12*, 758.
(32) Osman, M. A.; Seyfang, G.; Suter, U. W. *J. Phys. Chem B* **2000**, *104*, 4433.
(33) Casal, H. L.; Yang, P. W.; Mantsch, H. H. *Can. J. Chem.* **1986**, *64*, 1544.
(34) Hoffmann, H.; Mayer, U.; Brunner, H.; Krischanitz, A. *Vibr. Spectrosc.* **1995**, *8*, 151.
(35) Riou, S. A.; Chien, B. T.; Hsu, S. L.; Stidham, H. D. *J. Polym. Sci., Polym. Phys.* **1997**, *35*, 2843.
(36) Zhu, X.; Boiadjiev, V.; Mulder, J. A.; Hsung, R. P.; Major, R. C. *Langmuir* **2000**, *16*, 6766.
(37) Allara, D. L.; Parikh, A. N.; Rondelez, R. *Langmuir* **1995**, *11*, 2357.
(38) Grange, J. D. L.; Markham, J. L.; Kurkjian, C. R. *Langmuir* **1993**, *9*, 1749.
(39) Harder, P.; Grunze, M.; Dahint, R.; Whitesides, G. M.; Laibinis, P. E. *J. Phys. Chem. B* **1998**, *102*, 426.
(40) Valiokas, R.; Ostblom, M.; Svedhem, S.; Svensson, S. C. T.; Liedberg, B. *J. Phys. Chem. B* **2000**, *104*, 7565.
(41) Shimada, H.; Grutzner, J. B.; Kozlowski, J. F.; McLaughlin, J. L. *Biochemistry* **1998**, *37*, 854.
(42) Bryant, M. A.; Pemberton, J. E. *J. Am. Chem. Soc.* **1991**, *113*, 3629.
(43) Bryant, M. A.; Pemberton, J. E. *J. Am. Chem. Soc.* **1991**, *113*, 8284.
(44) Kim, Y.; Strauss, H. L.; Snyder, R. G. *J. Phys. Chem.* **1989**, *93*, 7520.
(45) Pemberton, J. E.; Cai, M. *Fresenius Anal. Chem.* **2001**, *369*, 328.
(46) Snyder, R. G.; Hsu, S. L.; Krimm, S. *Spectrochim. Acta* **1978**, *34A*, 395.
(47) Snyder, R. G.; Strauss, H. L.; Elliger, C. A. *J. Phys. Chem.* **1982**, *86*, 5145.
(48) Strobl, G. R.; Hagedorn, W. *J. Polym. Sci., Polym. Phys. Ed.* **1978**, *16*, 1181.
(49) Thompson, W. R.; Pemberton, J. E. *Anal. Chem.* **1994**, *66*, 3362.
(50) Wallace, B. A.; Blount, E. R. *Proc. Natl. Acad. Sci. U.S.A.* **1979**, *76*, 1775.
(51) Wunder, S. L. *Macromolecules* **1981**, *14*, 1024.
(52) Lin-Vien, J. G.; Colthup, N. B.; Fateley, W. G.; Grasselli, J. G. *The Handbook of Infrared and Raman Characteristic Frequencies of Organic Molecules*; Academic Press: New York, 1991.
(53) Harrand, M. *J. Chem. Phys.* **1983**, *79*, 5639.
(54) MacPhail, R. A.; Snyder, R. G.; Strauss, H. L. *J. Chem. Phys.* **1982**, *77*, 1118.
(55) Wallach, D. F. H.; Varma, S. P.; Fookson, J. *Biochim. Biophys. Acta* **1979**, *559*, 153.
(56) Larsson, K.; Rand, R. P. *Biochim. Biophys. Acta* **1973**, *326*, 245.
(57) Schoenfisch, M. H.; Pemberton, J. E. *Langmuir* **1999**, *15*, 509.
(58) Snyder, R. G.; Schachtschneider, J. H. *Spectrochim. Acta* **1963**, *19*, 117.
(59) Bower, D. I.; Maddams, W. F. *The Vibrational Spectroscopy of Polymers*; Cambridge University Press: New York, 1989.
(60) Abbate, S.; Zerbi, G.; Wunder, S. L. *J. Phys. Chem.* **1982**, *86*, 3140.
(61) Miranda, P. B.; Pflumio, V.; Saijo, H.; Shen, Y. R. *J. Am. Chem. Soc.* **1998**, *120*, 12092.
(62) Keller, A. *Philos. Mag.* **1957**, *2*, 1171.
(63) Niegisch, W. D.; Swan, P. R. *J. Appl. Phys.* **1960**, *31*, 1906.
(64) Shibukawa, T.; Gupta, V. D.; Turner, R.; Dillon, J. H.; Tobolsky, A. V. *Textile Res. J.* **1962**, 810.